Depth of maximum of air-shower profiles at the Pierre Auger Observatory.
II. Composition implications

A. Aab,[1] P. Abreu,[2] M. Aglietta,[3] E. J. Ahn,[4] I. Al Samarai,[5] I. F. M. Albuquerque,[6] I. Allekotte,[7] J. Allen,[8] P. Allison,[9] A. Almela,[10,11] J. Alvarez Castillo,[12] J. Alvarez-Muñiz,[13] R. Alves Batista,[14] M. Ambrosio,[15] A. Aminaei,[16] L. Anchordoqui,[17] S. Andringa,[2] C. Aramo,[15] V. M. Aranda,[18] F. Arqueros,[18] H. Asorey,[7] P. Assis,[2] J. Aublin,[19] M. Ave,[13] M. Avenier,[20] G. Avila,[21] N. Awal,[8] A. M. Badescu,[22] K. B. Barber,[23] J. Bäuml,[24] C. Baus,[24] J. J. Beatty,[9] K. H. Becker,[25] J. A. Bellido,[23] C. Berat,[20] M. E. Bertania,[3] X. Bertou,[7] P. L. Biermann,[26] P. Billoir,[19] S. Blaess,[23] M. Blanco,[19] C. Bleve,[27] H. Blümer,[24,28] M. Boháčová,[29] D. Boncioli,[30] C. Bonifazi,[31] R. Bonino,[3] N. Borodai,[32] J. Brack,[33] I. Brancus,[34] A. Bridgeman,[28] P. Brogueira,[2] W. C. Brown,[35] P. Buchholz,[1] A. Bueno,[36] S. Buitink,[16] M. Buscemi,[15] K. S. Caballero-Mora,[37] B. Caccianiga,[38] L. Caccianiga,[19] M. Candusso,[39] L. Caramete,[26] R. Caruso,[40] A. Castellina,[3] G. Cataldi,[27] L. Cazon,[2] R. Cester,[41] A. G. Chavez,[42] A. Chiavassa,[3] J. A. Chinellato,[43] J. Chudoba,[29] M. Cilmo,[15] R. W. Clay,[23] G. Cocciolo,[27] R. Colalillo,[15] A. Coleman,[44] L. Collica,[38] M. R. Coluccia,[27] R. Conceição,[2] F. Contreras,[45] M. J. Cooper,[23] A. Cordier,[46] S. Coutu,[44] C. E. Covault,[47] J. Cronin,[48] A. Curutiu,[26] R. Dallier,[49,50] B. Daniel,[43] S. Dasso,[51,52] K. Daumiller,[28] B. R. Dawson,[23] R. M. de Almeida,[53] M. De Domenico,[40] S. J. de Jong,[16,54] J. R. T. de Mello Neto,[31] I. De Mitri,[27] J. de Oliveira,[53] V. de Souza,[55] L. del Peral,[56] O. Deligny,[5] H. Dembinski,[28] N. Dhital,[57] C. Di Giulio,[39] A. Di Matteo,[58] J. C. Diaz,[57] M. L. Díaz Castro,[43] F. Diogo,[2] C. Dobrigkeit,[43] W. Docters,[59] J. C. D'Olivo,[12] A. Dorofeev,[33] Q. Dorosti Hasankiadeh,[28] M. T. Dova,[60] J. Ebr,[29] R. Engel,[28] M. Erdmann,[61] M. Erfani,[1] C. O. Escobar,[4,43] J. Espadanal,[2] A. Etchegoyen,[11,10] P. Facal San Luis,[48] H. Falcke,[16,62,54] K. Fang,[48] G. Farrar,[8] A. C. Fauth,[43] N. Fazzini,[4] A. P. Ferguson,[47] M. Fernandes,[31] B. Fick,[57] J. M. Figueira,[11] A. Filevich,[11] A. Filipčič,[63,64] B. D. Fox,[65] O. Fratu,[22] U. Fröhlich,[1] B. Fuchs,[24] T. Fuji,[48] R. Gaior,[19] B. García,[66] S. T. Garcia Roca,[13] D. Garcia-Gamez,[46] D. Garcia-Pinto,[18] G. Garilli,[40] A. Gascon Bravo,[36] F. Gate,[49] H. Gemmeke,[67] P. L. Ghia,[19] U. Giaccari,[31] M. Giammarchi,[38] M. Giller,[68] C. Glaser,[61] H. Glass,[4] M. Gómez Berisso,[7] P. F. Gómez Vitale,[21] P. Gonçalves,[2] J. G. Gonzalez,[24] N. González,[11] B. Gookin,[33] J. Gordon,[9] A. Gorgi,[3] P. Gorham,[65] P. Gouffon,[6] S. Grebe,[16,54] N. Griffith,[9] A. F. Grillo,[30] T. D. Grubb,[23] F. Guarino,[15] G. P. Guedes,[69] M. R. Hampel,[11] P. Hansen,[60] D. Harari,[7] T. A. Harrison,[23] S. Hartmann,[61] J. L. Harton,[33] A. Haungs,[28] T. Hebbeker,[61] D. Heck,[28] P. Heimann,[1] A. E. Herve,[28] G. C. Hill,[23] C. Hojvat,[4] N. Hollon,[48] E. Holt,[28] P. Homola,[25] J. R. Hörandel,[16,54] P. Horvath,[70] M. Hrabovský,[70,29] D. Huber,[24] T. Huege,[28] A. Insolia,[40] P. G. Isar,[71] I. Jandt,[25] S. Jansen,[16,54] C. Jarne,[60] M. Josebachuili,[11] A. Kääpä,[25] O. Kambeitz,[24] K. H. Kampert,[25] P. Kasper,[4] I. Katkov,[24] B. Kégl,[46] B. Keilhauer,[28] A. Keivani,[44] E. Kemp,[43] R. M. Kieckhafer,[57] H. O. Klages,[28] M. Kleifges,[67] J. Kleinfeller,[45] R. Krause,[61] N. Krohm,[25] O. Krömer,[67] D. Kruppke-Hansen,[25] D. Kuempel,[61] N. Kunka,[67] D. LaHurd,[47] L. Latronico,[3] R. Lauer,[72] M. Lauscher,[61] P. Lautridou,[49] S. Le Coz,[20] M. S. A. B. Leão,[73] D. Lebrun,[20] P. Lebrun,[4] M. A. Leigui de Oliveira,[74] A. Letessier-Selvon,[19] I. Lhenry-Yvon,[5] K. Link,[24] R. López,[75] A. Lopez Agüera,[13] K. Louedec,[20] J. Lozano Bahilo,[36] L. Lu,[25,76] A. Lucero,[11] M. Ludwig,[24] M. Malacari,[23] S. Maldera,[3] M. Mallamaci,[38] J. Maller,[49] D. Mandat,[29] P. Mantsch,[4] A. G. Mariazzi,[60] V. Marin,[49] I. C. Mariş,[36] G. Marsella,[27] D. Martello,[27] L. Martin,[49,50] H. Martinez,[37] O. Martínez Bravo,[75] D. Martraire,[5] J. J. Masías Meza,[52] H. J. Mathes,[28] S. Mathys,[25] J. Matthews,[77] J. A. J. Matthews,[72] G. Matthiae,[39] D. Maurel,[24] D. Maurizio,[78] E. Mayotte,[79] P. O. Mazur,[4] C. Medina,[79] G. Medina-Tanco,[12] R. Meissner,[61] M. Melissas,[24] D. Melo,[11] A. Menshikov,[67] S. Messina,[59] R. Meyhandan,[65] S. Mićanović,[80] M. I. Micheletti,[81] L. Middendorf,[61] I. A. Minaya,[18] L. Miramonti,[38] B. Mitrica,[34] L. Molina-Bueno,[36] S. Mollerach,[7] M. Monasor,[48] D. Monnier Ragaigne,[46] F. Montanet,[20] C. Morello,[3] M. Mostafá,[44] C. A. Moura,[74] M. A. Muller,[43,82] G. Müller,[61] S. Müller,[28] M. Münchmeyer,[19] R. Mussa,[41] G. Navarra,[3] S. Navas,[36] P. Necesal,[29] L. Nellen,[12] A. Nelles,[16,54] J. Neuser,[25] P. Nguyen,[23] M. Niechciol,[1] L. Niemietz,[25] T. Niggemann,[61] D. Nitz,[57] D. Nosek,[83] V. Novotny,[83] L. Nožka,[70] A. Olinto,[48] M. Oliveira,[2] N. Pacheco,[56] D. Pakk Selmi-Dei,[43] M. Palatka,[29] J. Pallotta,[84] N. Palmieri,[24] P. Papenbreer,[25] G. Parente,[13] A. Parra,[13] T. Paul,[17,85] M. Pech,[29] J. Pękala,[32] R. Pelayo,[75] I. M. Pepe,[86] L. Perrone,[27] E. Petermann,[87] C. Peters,[61] S. Petrera,[58,88] Y. Petrov,[33] J. Phuntsok,[44] R. Piegaia,[52] T. Pierog,[28] P. Pieroni,[52] M. Pimenta,[2] V. Pirronello,[40] M. Platino,[11] M. Plum,[61] A. Porcelli,[28] C. Porowski,[32] R. R. Prado,[55] P. Privitera,[48] M. Prouza,[29] V. Purrello,[7] E. J. Quel,[84] S. Querchfeld,[25] S. Quinn,[47] J. Rautenberg,[25] O. Ravel,[49] D. Ravignani,[11] B. Revenu,[49] J. Ridky,[29] S. Riggi,[89,13] M. Risse,[1] P. Ristori,[84] V. Rizi,[58] W. Rodrigues de Carvalho,[13] I. Rodriguez Cabo,[13] G. Rodriguez Fernandez,[39,13] J. Rodriguez Rojo,[45] M. D. Rodríguez-Frías,[56] D. Rogozin,[28] G. Ros,[56] J. Rosado,[18] T. Rossler,[70] M. Roth,[28] E. Roulet,[7] A. C. Rovero,[51] S. J. Saffi,[23] A. Saftoiu,[34] F. Salamida,[5] H. Salazar,[75] A. Saleh,[64] F. Salesa Greus,[44] G. Salina,[39] F. Sánchez,[11] P. Sanchez-Lucas,[36] C. E. Santo,[2] E. Santos,[43] E. M. Santos,[6] F. Sarazin,[79] B. Sarkar,[25] R. Sarmento,[2] R. Sato,[45] N. Scharf,[61] V. Scherini,[27] H. Schieler,[28] P. Schiffer,[14] D. Schmidt,[28] O. Scholten,[59] H. Schoorlemmer,[65,16,54] P. Schovánek,[29] A. Schulz,[28] J. Schulz,[16] J. Schumacher,[61] S. J. Sciutto,[60] A. Segreto,[89] M. Settimo,[19] A. Shadkam,[77] R. C. Shellard,[78] I. Sidelnik,[7] G. Sigl,[14] O. Sima,[90] A. Śmiałkowski,[68] R. Šmída,[28] G. R. Snow,[87] P. Sommers,[44] J. Sorokin,[23] R. Squartini,[45] Y. N. Srivastava,[85] S. Stanič,[64] J. Stapleton,[9] J. Stasielak,[32] M. Stephan,[61] A. Stutz,[20] F. Suarez,[11] T. Suomijärvi,[5] A. D. Supanitsky,[51] M. S. Sutherland,[9] J. Swain,[85] Z. Szadkowski,[68] M. Szuba,[28] O. A. Taborda,[7] A. Tapia,[11] M. Tartare,[20]

A. Tepe,[1] V. M. Theodoro,[43] C. Timmermans,[54,16] C. J. Todero Peixoto,[91] G. Toma,[34] L. Tomankova,[28] B. Tomé,[2] A. Tonachini,[41] G. Torralba Elipe,[13] D. Torres Machado,[31] P. Travnicek,[29] E. Trovato,[40] M. Tueros,[13] R. Ulrich,[28] M. Unger,[28] M. Urban,[61] J. F. Valdés Galicia,[12] I. Valiño,[13] L. Valore,[15] G. van Aar,[16] P. van Bodegom,[23] A. M. van den Berg,[59] S. van Velzen,[16] A. van Vliet,[14] E. Varela,[75] B. Vargas Cárdenas,[12] G. Varner,[65] J. R. Vázquez,[18] R. A. Vázquez,[13] D. Veberič,[46] V. Verzi,[39] J. Vicha,[29] M. Videla,[11] L. Villaseñor,[42] B. Vlcek,[56] S. Vorobiov,[64] H. Wahlberg,[60] O. Wainberg,[11,10] D. Walz,[61] A. A. Watson,[76] M. Weber,[67] K. Weidenhaupt,[61] A. Weindl,[28] F. Werner,[24] A. Widom,[85] L. Wiencke,[79] B. Wilczyńska,[32] H. Wilczyński,[32] M. Will,[28] C. Williams,[48] T. Winchen,[25] D. Wittkowski,[25] B. Wundheiler,[11] S. Wykes,[16] T. Yamamoto,[48] T. Yapici,[57] G. Yuan,[77] A. Yushkov,[1] B. Zamorano,[36] E. Zas,[13] D. Zavrtanik,[64,63] M. Zavrtanik,[63,64] I. Zaw,[8] A. Zepeda,[37] J. Zhou,[48] Y. Zhu,[67] M. Zimbres Silva,[43] M. Ziolkowski,[1] and F. Zuccarello[40]

(Pierre Auger Collaboration)[*]

[1]*Universität Siegen, Siegen, Germany*
[2]*Laboratório de Instrumentação e Física Experimental de Partículas (LIP) and Instituto Superior Técnico (IST), Universidade de Lisboa (UL), Portugal*
[3]*Osservatorio Astrofisico di Torino (INAF), Università di Torino and Sezione INFN, Torino, Italy*
[4]*Fermilab, Batavia, Illinois, USA*
[5]*Institut de Physique Nucléaire d'Orsay (IPNO), Université Paris 11, CNRS-IN2P3, Orsay, France*
[6]*Universidade de São Paulo, Instituto de Física, São Paulo, São Paulo, Brazil*
[7]*Centro Atómico Bariloche and Instituto Balseiro (CNEA-UNCuyo-CONICET), San Carlos de Bariloche, Argentina*
[8]*New York University, New York, New York, USA*
[9]*Ohio State University, Columbus, Ohio, USA*
[10]*Universidad Tecnológica Nacional-Facultad Regional Buenos Aires,, Buenos Aires, Argentina*
[11]*Instituto de Tecnologías en Detección y Astropartículas (CNEA, CONICET, UNSAM), Buenos Aires, Argentina*
[12]*Universidad Nacional Autonoma de Mexico, Mexico, Distrito Federal, Mexico*
[13]*Universidad de Santiago de Compostela, Spain*
[14]*Universität Hamburg, Hamburg, Germany*
[15]*Università di Napoli "Federico II" and Sezione INFN, Napoli, Italy*
[16]*IMAPP, Radboud University, Nijmegen, Netherlands*
[17]*Department of Physics and Astronomy, Lehman College, City University of New York, New York, USA*
[18]*Universidad Complutense de Madrid, Madrid, Spain*
[19]*Laboratoire de Physique Nucléaire et de Hautes Energies (LPNHE), Universités Paris 6 et Paris 7, CNRS-IN2P3 Paris, France*
[20]*Laboratoire de Physique Subatomique et de Cosmologie (LPSC), Université Grenoble-Alpes, CNRS/IN2P3, France*
[21]*Observatorio Pierre Auger and Comisión Nacional de Energía Atómica, Malargüe, Argentina*
[22]*University Politehnica of Bucharest, Romania*
[23]*University of Adelaide, Adelaide, South Australia, Australia*
[24]*Karlsruhe Institute of Technology—Campus South—Institut für Experimentelle Kernphysik (IEKP), Karlsruhe, Germany*
[25]*Bergische Universität Wuppertal, Wuppertal, Germany*
[26]*Max-Planck-Institut für Radioastronomie, Bonn, Germany*
[27]*Dipartimento di Matematica e Fisica "E. De Giorgi" dell'Università del Salento and Sezione INFN, Lecce, Italy*
[28]*Karlsruhe Institute of Technology—Campus North—Institut für Kernphysik, Karlsruhe, Germany*
[29]*Institute of Physics of the Academy of Sciences of the Czech Republic, Prague, Czech Republic*
[30]*INFN, Laboratori Nazionali del Gran Sasso, Assergi (L'Aquila), Italy*
[31]*Universidade Federal do Rio de Janeiro, Instituto de Física, Rio de Janeiro, Rio de Janeiro, Brazil*
[32]*Institute of Nuclear Physics PAN, Krakow, Poland*
[33]*Colorado State University, Fort Collins, Colorado, USA*
[34]*'Horia Hulubei' National Institute for Physics and Nuclear Engineering, Bucharest-Magurele, Romania*
[35]*Colorado State University, Pueblo, Colorado, USA*
[36]*Universidad de Granada and C.A.F.P.E., Granada, Spain*
[37]*Centro de Investigación y de Estudios Avanzados del IPN (CINVESTAV), México, Distrito Federal, Mexico*
[38]*Università di Milano and Sezione INFN, Milan, Italy*
[39]*Università di Roma II "Tor Vergata" and Sezione INFN, Roma, Italy*

[40]*Università di Catania and Sezione INFN, Catania, Italy*
[41]*Università di Torino and Sezione INFN, Torino, Italy*
[42]*Universidad Michoacana de San Nicolas de Hidalgo, Morelia, Michoacan, Mexico*
[43]*Universidade Estadual de Campinas, IFGW, Campinas, São Paulo, Brazil*
[44]*Pennsylvania State University, University Park, USA*
[45]*Observatorio Pierre Auger, Malargüe, Argentina*
[46]*Laboratoire de l'Accélérateur Linéaire (LAL), Université Paris 11, CNRS-IN2P3 Orsay, France*
[47]*Case Western Reserve University, Cleveland, Ohio, USA*
[48]*University of Chicago, Enrico Fermi Institute, Chicago, Illinois, USA*
[49]*SUBATECH, École des Mines de Nantes, CNRS-IN2P3, Université de Nantes, Nantes, France*
[50]*Station de Radioastronomie de Nançay, Observatoire de Paris, CNRS/INSU Nançay, France*
[51]*Instituto de Astronomía y Física del Espacio (CONICET-UBA), Buenos Aires, Argentina*
[52]*Departamento de Física, FCEyN, Universidad de Buenos Aires y CONICET, Argentina*
[53]*Universidade Federal Fluminense, EEIMVR, Volta Redonda, Rio de Janeiro, Brazil*
[54]*Nikhef, Science Park, Amsterdam, Netherlands*
[55]*Universidade de São Paulo, Instituto de Física de São Carlos, São Carlos, São Paulo, Brazil*
[56]*Universidad de Alcalá, Alcalá de Henares, Spain*
[57]*Michigan Technological University, Houghton, Michigan, USA*
[58]*Dipartimento di Scienze Fisiche e Chimiche dell'Università dell'Aquila and INFN, Italy*
[59]*KVI, Center for Advanced Radiation Technology, University of Groningen, Groningen, Netherlands*
[60]*IFLP, Universidad Nacional de La Plata and CONICET, La Plata, Argentina*
[61]*RWTH Aachen University, III. Physikalisches Institut A, Aachen, Germany*
[62]*ASTRON, Dwingeloo, Netherlands*
[63]*Experimental Particle Physics Department, J. Stefan Institute, Ljubljana, Slovenia*
[64]*Laboratory for Astroparticle Physics, University of Nova Gorica, Slovenia*
[65]*University of Hawaii, Honolulu, Hawaii, USA*
[66]*Instituto de Tecnologías en Detección y Astropartículas (CNEA, CONICET, UNSAM) and National Technological University, Faculty Mendoza (CONICET/CNEA), Mendoza, Argentina*
[67]*Karlsruhe Institute of Technology—Campus North—Institut für Prozessdatenverarbeitung und Elektronik, Germany*
[68]*University of Łódź, Łódź, Poland*
[69]*Universidade Estadual de Feira de Santana, Brazil*
[70]*Palacky University, RCPTM, Olomouc, Czech Republic*
[71]*Institute of Space Sciences, Bucharest, Romania*
[72]*University of New Mexico, Albuquerque, New Mexico, USA*
[73]*Faculdade Independente do Nordeste, Vitória da Conquista, Brazil*
[74]*Universidade Federal do ABC, Santo André, São Paulo, Brazil*
[75]*Benemérita Universidad Autónoma de Puebla, Mexico*
[76]*School of Physics and Astronomy, University of Leeds, United Kingdom*
[77]*Louisiana State University, Baton Rouge, Louisiana, USA*
[78]*Centro Brasileiro de Pesquisas Fisicas, Rio de Janeiro, Rio de Janeiro, Brazil*
[79]*Colorado School of Mines, Golden, Colorado, USA*
[80]*Rudjer Bošković Institute, 10000 Zagreb, Croatia*
[81]*Instituto de Física de Rosario (IFIR)—CONICET/U.N.R. and Facultad de Ciencias Bioquímicas y Farmacéuticas U.N.R., Rosario, Argentina*
[82]*Universidade Federal de Pelotas, Pelotas, Rio Grande do Sul, Brazil*
[83]*Charles University, Faculty of Mathematics and Physics, Institute of Particle and Nuclear Physics, Prague, Czech Republic*
[84]*Centro de Investigaciones en Láseres y Aplicaciones, CITEDEF and CONICET, Argentina*
[85]*Northeastern University, Boston, Massachusetts, USA*
[86]*Universidade Federal da Bahia, Salvador, Bahia, Brazil*
[87]*University of Nebraska, Lincoln, Nebraska, USA*
[88]*Gran Sasso Science Institute (INFN), L'Aquila, Italy*
[89]*Istituto di Astrofisica Spaziale e Fisica Cosmica di Palermo (INAF), Palermo, Italy*
[90]*University of Bucharest, Physics Department, Romania*
[91]*Universidade de São Paulo, Escola de Engenharia de Lorena, Lorena, São Paulo, Brazil*

[*]auger_spokespersons@fnal.gov

Using the data taken at the Pierre Auger Observatory between December 2004 and December 2012, we have examined the implications of the distributions of depths of atmospheric shower maximum ($X_{\max}$), using a hybrid technique, for composition and hadronic interaction models. We do this by fitting the distributions with predictions from a variety of hadronic interaction models for variations in the composition of the primary cosmic rays and examining the quality of the fit. Regardless of what interaction model is assumed, we find that our data are not well described by a mix of protons and iron nuclei over most of the energy range. Acceptable fits can be obtained when intermediate masses are included, and when this is done consistent results for the proton and iron-nuclei contributions can be found using the available models. We observe a strong energy dependence of the resulting proton fractions, and find no support from any of the models for a significant contribution from iron nuclei. However, we also observe a significant disagreement between the models with respect to the relative contributions of the intermediate components.

I. INTRODUCTION

The composition of ultra–high energy cosmic rays (UHECRs) is an important input for elucidating their origin that has yet to be fully understood. The atmospheric depth where the longitudinal development of an air shower reaches the maximum number of particles, $X_{\max}$, is a standard parameter used to extract composition information as different nuclei produce different distributions of $X_{\max}$ [1]. The mean and dispersion of $X_{\max}$ have been previously [2] utilized to infer information on the composition, especially since the former scales linearly with the logarithm of the composition mass $\ln A$. Data taken at the Pierre Auger Observatory [3] located in Argentina are well suited to study composition as the capabilities of the observatory for hybrid[1] detection of air showers enable high-accuracy measurement of the $X_{\max}$ parameter [4].

In a recent study [5], the mean and dispersion of $X_{\max}$ were converted to the first two moments of the $\ln A$ distribution to deduce the details of the mass composition extracted from the Auger data. That method allowed us to obtain the average logarithmic mass of components that describe the data, as well as testing if that combination is feasible for the given hadronic interaction model used. In this work, we use the shape of the distribution of $X_{\max}$ data from Auger to infer the composition. Using the $X_{\max}$ distribution maximizes the information and helps reduce degeneracies that can occur when one considers only the first two moments of the $X_{\max}$ distribution. Figure 1 displays two simulated distributions with different mixes of composition but with identical means and dispersions. By maintaining sensitivity to the shape of the distribution, information on the composition can be retrieved that goes beyond the mean and dispersion of $\ln A$.

For a given hadronic interaction model, the $X_{\max}$ distribution is compared to predictions made using Monte Carlo (MC) simulations formed with varying nuclear fractions, and a binned maximum-likelihood discriminator is used to choose the best-fit fractions. This method also allows us to obtain information on the goodness of the fit.

The hybrid $X_{\max}$ data set in the range $E = 10^{17.8}$–10^{20} eV measured by Auger [4] is used to determine whether it can be described satisfactorily by an evolution of composition with energy. We first consider a mixture of the two most stable types of particles, protons, and iron nuclei, and then we extend the fits to include extra components. Specifically, we include helium and nitrogen nuclei as representatives of the intermediate range of nuclear masses.

The procedure used to form the MC predictions is described in Sec. II, and the fitting procedure is described in Sec. III. The systematics considered in the analysis are described in Sec. IV, the results are presented in Sec. V, and the discussion and conclusions in Sec. VI.

II. TEMPLATES FOR MONTE CARLO SIMULATIONS OF $X_{\max}$

A template is developed for the MC simulation of the $X_{\max}$ distribution for a single nuclear species, and is created to compare it with the data. To form a template, we start with the true $X_{\max}$ obtained from events generated in the MC with specific incident species and a given energy range. To generate the simulations, the algorithm CONEX v4r37 [6,7] has been used to simulate air showers, using the three most common hadronic interaction packages EPOS-LHC [8], QGSJet II-4 [9], and Sibyll 2.1 [10], where the first two models have been updated with the $E_{\mathrm{CM}} = 7$ TeV LHC data.

There are 2×10^4 showers simulated per species per energy bin. The zenith angle is distributed isotropically on a flat surface ($dN/d\cos(\theta) \sim \cos\theta$) between 0 and 80 degrees. The distribution of energy within a given bin
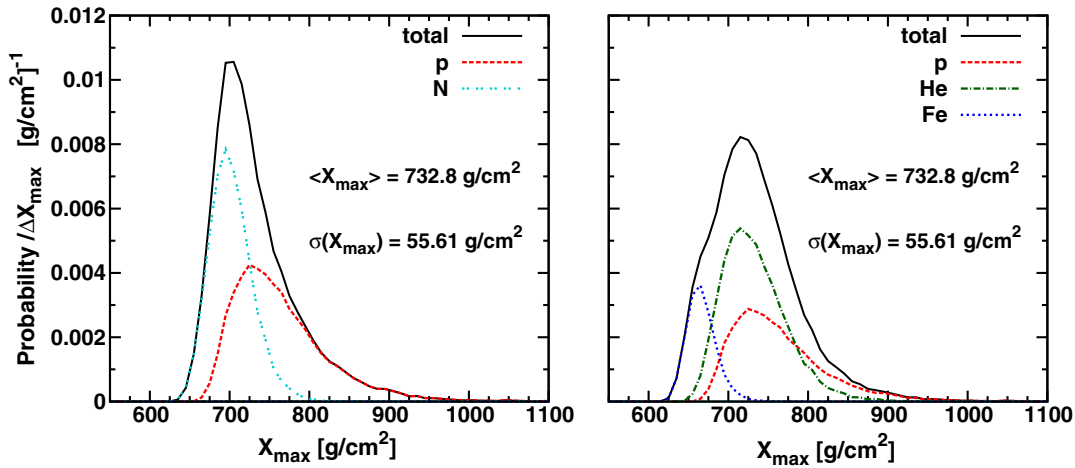
---

[1]These are events that triggered both the surface and fluorescence detectors. The surface detectors are used to constrain shower geometry and thereby to reduce the uncertainty in the $X_{\max}$ reconstruction.

FIG. 1 (color online). Two X_{max} distributions generated with identical mean and dispersion but with different compositions. The hadronic interaction model EPOS-LHC was used to generate 10^4 events in the range $E = 10^{18.2-18.3}$ eV.

follows E^{-a}, where $a = 1.1$ or 2.2 for energies below or above 10^{18} eV, respectively.[2]

The true X_{max} for a given nuclear species s, X_s^t, is determined by a quadratic interpolation around the peak as a function of slant depth. The template is a binned X_{max} distribution that includes effects of acceptance and measurement resolution. The content of the jth bin is the sum of the contributions from the N_{MC} simulated events, each weighted by the acceptance;

$$X_{s,j}^m = \sum_n^{N_{MC}} a(X_{s,n}^t) p_j(X_{s,n}^t)/N_{MC}, \qquad (1)$$

where $a(X_{s,n}^t)$ is the acceptance weight for the nth event and $p_j(X_{s,n}^t)$ is the probability that X_{max} measured for this event lies within the range defined by the jth bin. This probability is obtained assuming a resolution function represented by a double Gaussian, where the parameters of the dependence on energy have been determined using a full detector simulation [4]. Note that $a(X_{s,n}^t)$ is not included in the normalization of the template so that the sum of $X_{s,j}^m$ is somewhat less than 1 by an amount depending on the overall acceptance for a given species arriving within the field of view. This overall factor to correct for acceptance ranges from 0.979 for protons in the EPOS-LHC model, and up to 1 for iron nuclei in all models.

---

[2]This parametrization was derived from the energy distribution of preliminary data, whereas the current data set is best described by $a = 1.76 + 0.44 \log E/\mathrm{EeV}$ [4]. The new parametrization would produce at most a 0.3% shift in the average energy within a bin, which is negligible when compared to the systematic energy-scale uncertainty.

III. FITTING PROCEDURE

We use hybrid data collected with Auger between December 2004 and December 2012, where 19,759 events survived all the cuts with energies of $E_{lab} = 10^{17.8}$ eV and higher, as described in Ref. [4]. The events are binned in intervals of 0.1 in $\log(E/\mathrm{eV})$ from $10^{17.8}$ to $10^{19.5}$ eV and events with energy above $10^{19.5}$ eV are combined into one bin. The number of events ranges from more than 3000 per low-energy bin to about 40 for the highest-energy bin. The X_{max} bins are defined to be 20 g/cm^2 wide starting at $X_{max} = 0$.

To carry out the comparison with data, for a given energy bin the template $X_{s,j}^m$ for each species is weighted according to its species fraction f_s and combined to form MC predictions, C_j, for each X_{max} bin:

$$C_j = \frac{N_{data}}{N} \sum_s f_s X_{s,j}^m, \qquad (2)$$

where N_{data} is the number of measured events in the energy bin and the normalization term N is a function of f_s,

$$N = \sum_s f_s \sum_j^\infty X_{s,j}^m, \qquad (3a)$$

with

$$\sum_s f_s = 1. \qquad (3b)$$

We use the normalizations for the templates and for the predictions to interpret f_s as the fraction of species s at the top of the atmosphere, i.e., without the need to correct for detector acceptance.
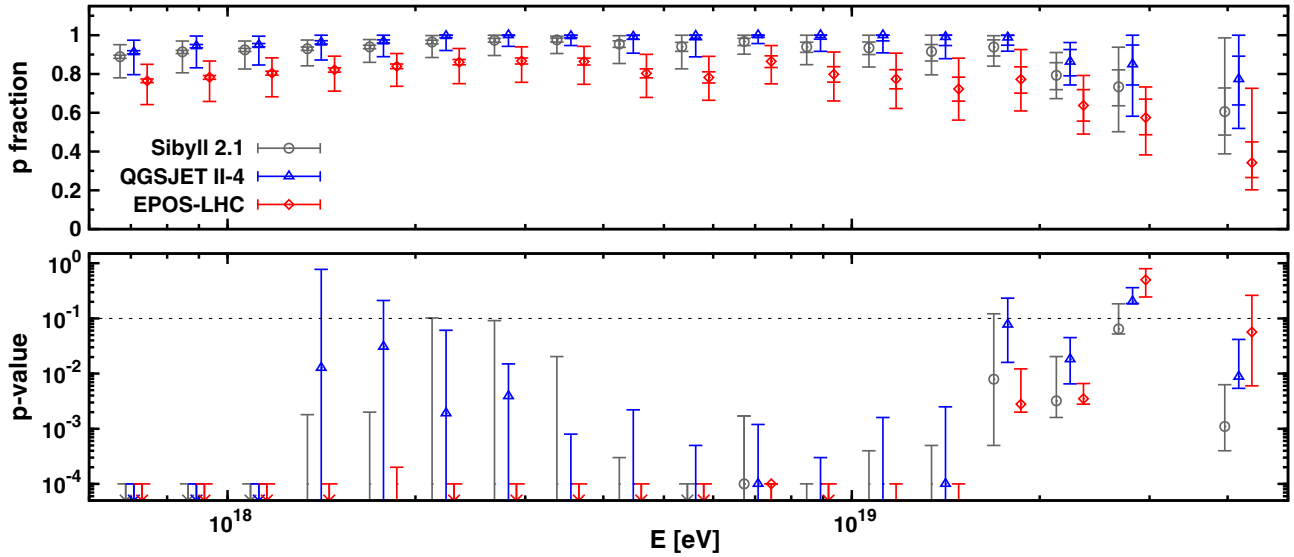
FIG. 2 (color online). Fitted fraction and quality for the scenario with protons and iron nuclei only. The upper panel shows the proton fraction and the lower panel shows the *p*-values. The horizontal dotted line in the lower panel indicates $p = 0.1$. The results from the various hadronic interaction models are slightly shifted in energy for better viewing (Sibyll 2.1 to the left, EPOS-LHC to the right).
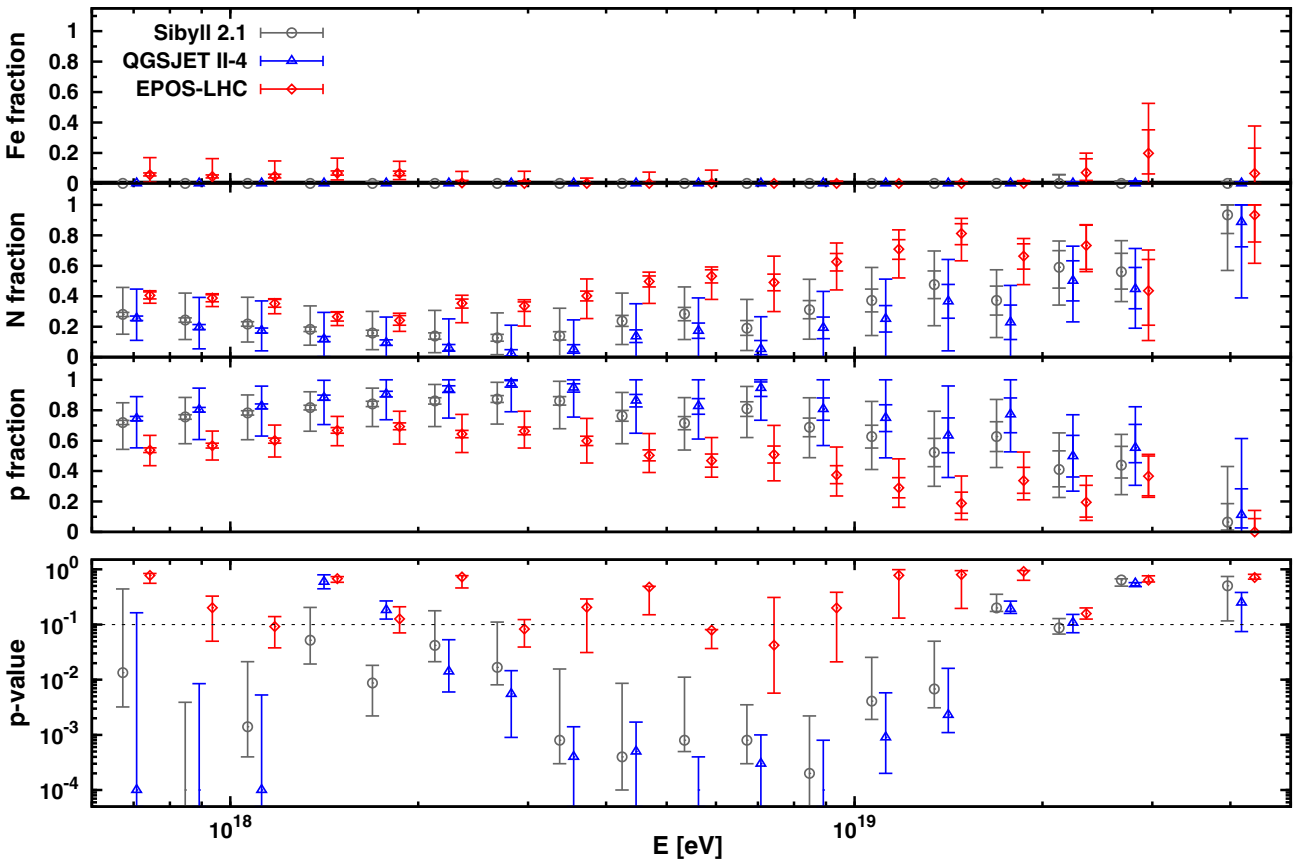

FIG. 3 (color online). Fitted fraction and quality for the scenario of a complex mixture of protons, nitrogen nuclei, and iron nuclei. The upper panels show the species fractions and the lower panel shows the *p*-values.

A binned maximum-likelihood method is used to find the best-fitting combination of the various species. For a given energy bin E, the likelihood is expressed as

$$L = \prod_j \left[\frac{e^{-C_j} C_j^{n_j}}{n_j!} \right], \qquad (4)$$

where n_j is the measured count of events in $X_{\max}$ bin j and C_j is the corresponding MC prediction. As a practical consideration, we remove the factorials by dividing L by the likelihood value obtained when $C_j = n_j$. As this value is a constant factor, the maximization is not affected by this process. This has the added advantage that the resulting likelihood ratio can also be used as an estimator for the goodness of fit [11];

$$L\prime = \prod_j \left[\frac{e^{-C_j} C_j^{n_j}}{n_j!} \right] \Big/ \left[\frac{e^{-n_j} n_j^{n_j}}{n_j!} \right]. \qquad (5)$$

The species fractions F_i that best fit the data are found by minimizing the negative log-likelihood expression

$$\mathcal{L} = -\ln L\prime = \sum_j \left(C_j - n_j + n_j \ln \frac{n_j}{C_j} \right). \qquad (6)$$

The fit quality is measured by the p-value, which is defined as the probability of obtaining a worse fit (larger $\mathcal{L}$) than that obtained with the data, assuming that the distribution predicted by the fit results is correct. To construct p-values for the fit, mock data sets of the predicted $X_{\max}$ distribution were generated from the templates with size equal to the real data set. The p-value was calculated as the fraction of mock data sets
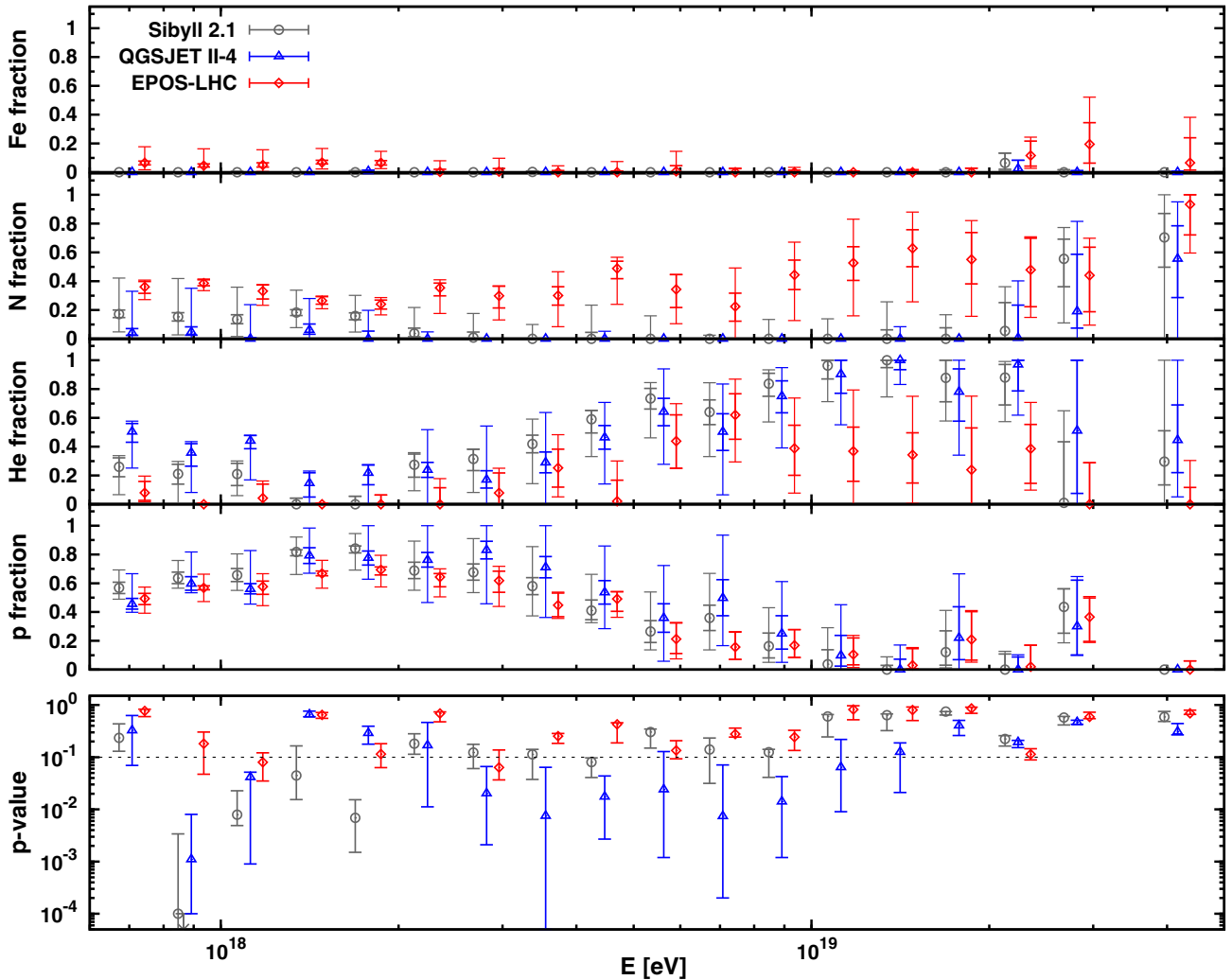
FIG. 4 (color online). Fitted fraction and quality for the scenario of a complex mixture of protons, helium nuclei, nitrogen nuclei, and iron nuclei. The upper panels show the species fractions and the lower panel shows the p-values.

with $\mathcal{L}$ worse than that obtained from the real data. Since the parameters in the fit are constrained by both physical and unitarity bounds, we do not expect $\mathcal{L}$ to necessarily behave like a χ^2 variable and hence do not use the $\Delta \mathcal{L} = 1/2$ rule to obtain the statistical uncertainty on the fit parameters. Instead, the statistical uncertainty for each species has been determined by using a generalization of the Feldman-Cousins procedure [12]. Known as the profile-likelihood method [13], a multidimensional likelihood function is reduced to a function that only depends on the parameter of prime interest. The 68% confidence range for each species fraction is determined through this method by treating the other species fractions as nuisance parameters. The method properly

accounts for correlations and provides a smooth transition from two-sided bounds to one-sided limits.

IV. SYSTEMATIC UNCERTAINTIES

The most important source of systematic uncertainty considered is that on X_{max}^m itself as determined in Ref. [4]. The effect of this uncertainty on the fit fractions is determined by fitting the data with model predictions shifted in X_{max} by an amount δX_{max}. The models are shifted rather than the data in order to avoid statistical artifacts resulting from rebinning of the data. Since we do not expect the fit fractions to evolve monotonically with respect to δX_{max}, we scan δX_{max} between $+1\sigma$ and -1σ in
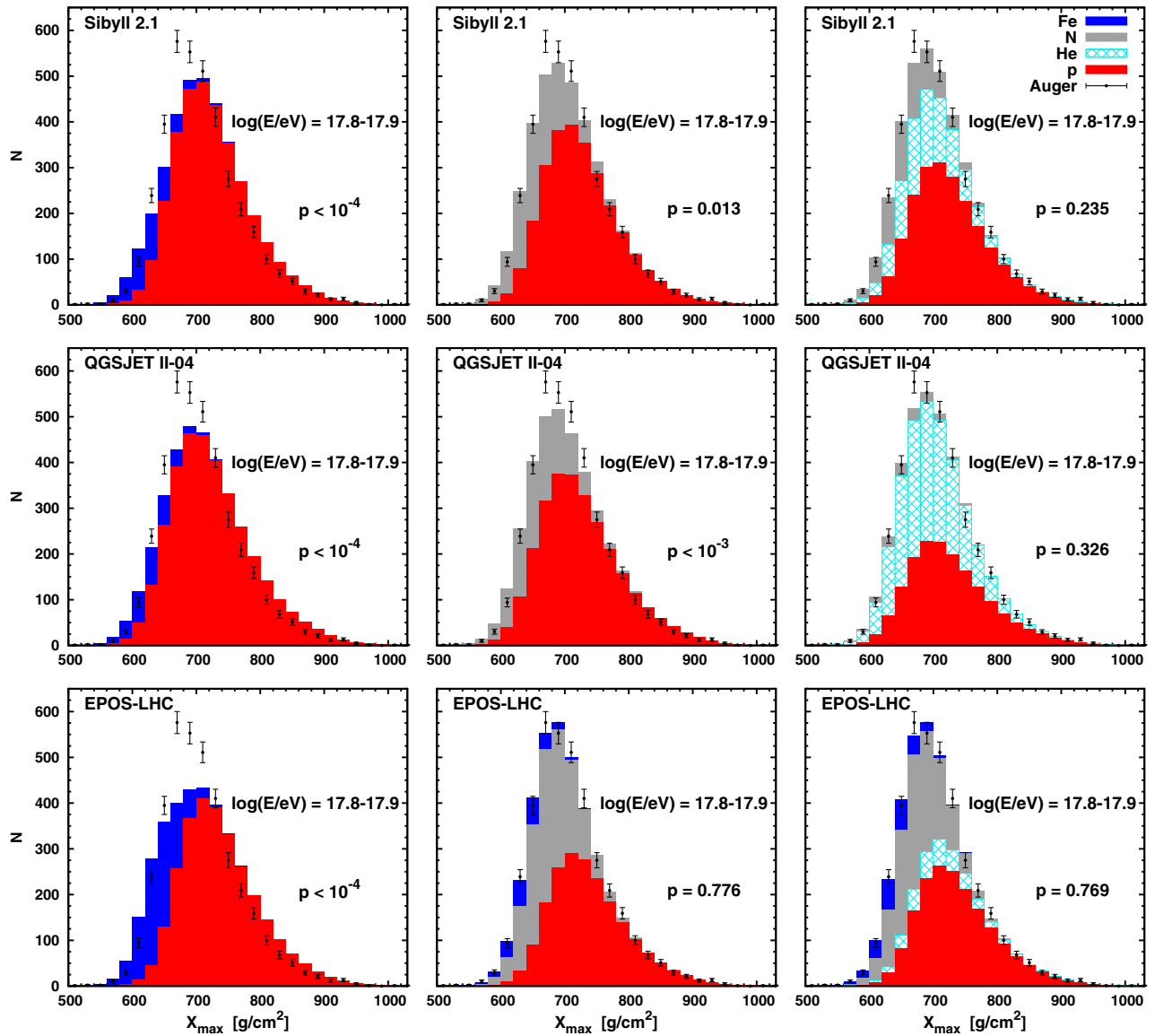
FIG. 5 (color online). X_{max} distribution of the fits for energy bin $E = 10^{17.8-17.9}$ eV. Results using Sibyll 2.1 are shown in the top row, QGSJET II-4 in the middle row, and EPOS-LHC in the bottom row. The left column displays results where protons and iron nuclei were used, the central column also includes nitrogen nuclei, and the right column includes helium nuclei in addition.

steps of 0.2σ in order to determine the maximum range over which a fit fraction can vary.

The other possible systematic uncertainties we considered are those on the energy scale and on the parametrization of the resolution functions for acceptance and X_{max}. The effect of the parametrization uncertainties is evaluated by refitting the data with extreme values of the parametrizations. The latter values were chosen to produce the largest or smallest acceptance or resolution, respectively, compatible with the data [4]. None of the parametrization variants resulted in significant changes to the fit fractions. Since the uncertainty in the energy scale is comparable to the width of the energy bin, we evaluated its effect by simply refitting the data with MC templates constructed from adjacent energy bins. The effects on the fit fractions were similar to, but generally smaller than, the shifts in X_{max} scale.

The overall systematic uncertainty assigned to a given fit fraction is chosen to encompass the full range of values obtained by any of the fit variants described above. The p-values are also calculated for each of these fit variants in order to assess their effect on the goodness of fit.

V. RESULTS

The fit result for the mix of protons and iron nuclei is shown in Fig. 2. Fit results with additional components are shown in Figs. 3 and 4. For each figure the species fractions are shown in the upper panel(s). Only the proton fraction is shown for the combination of protons and iron nuclei
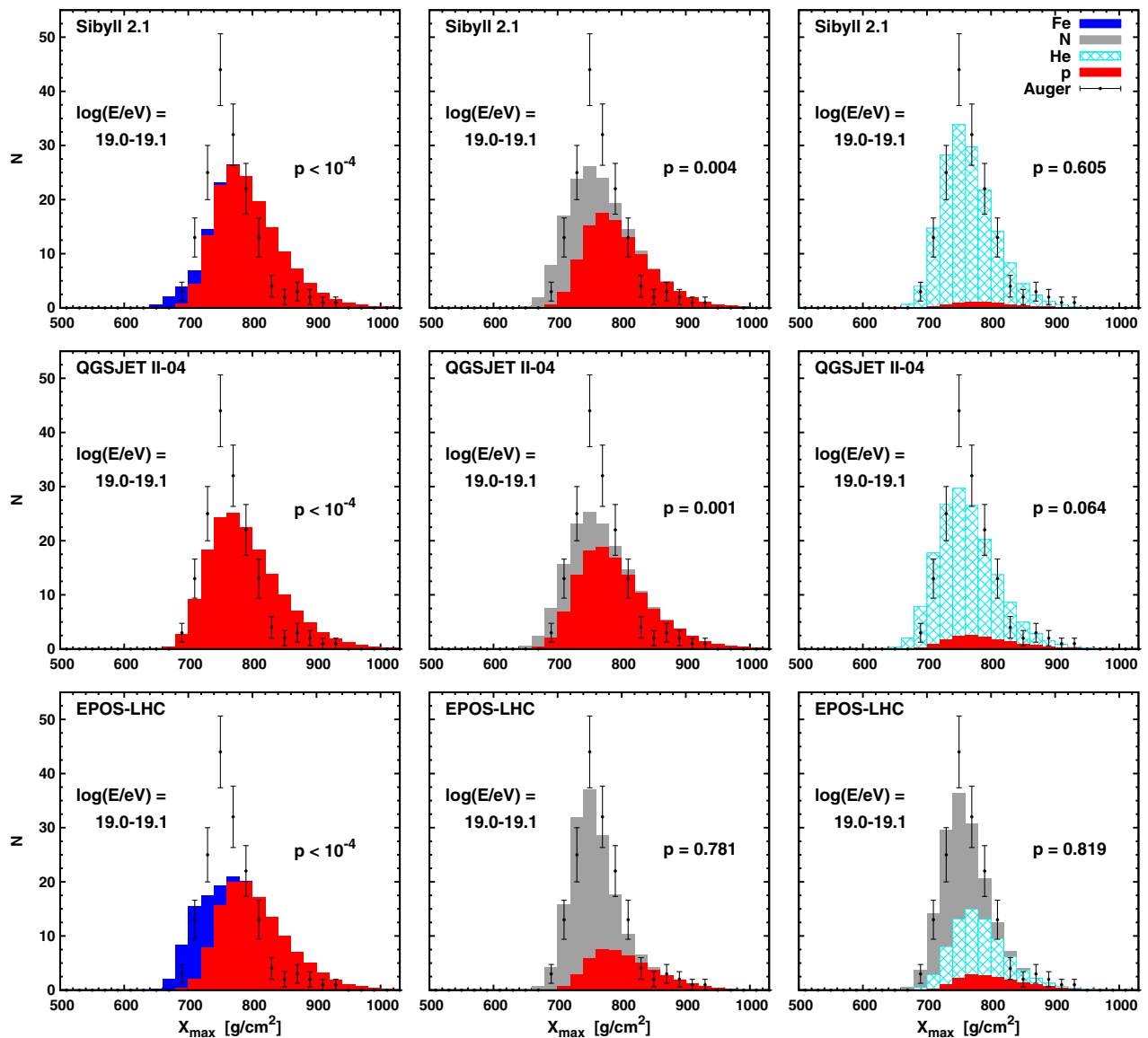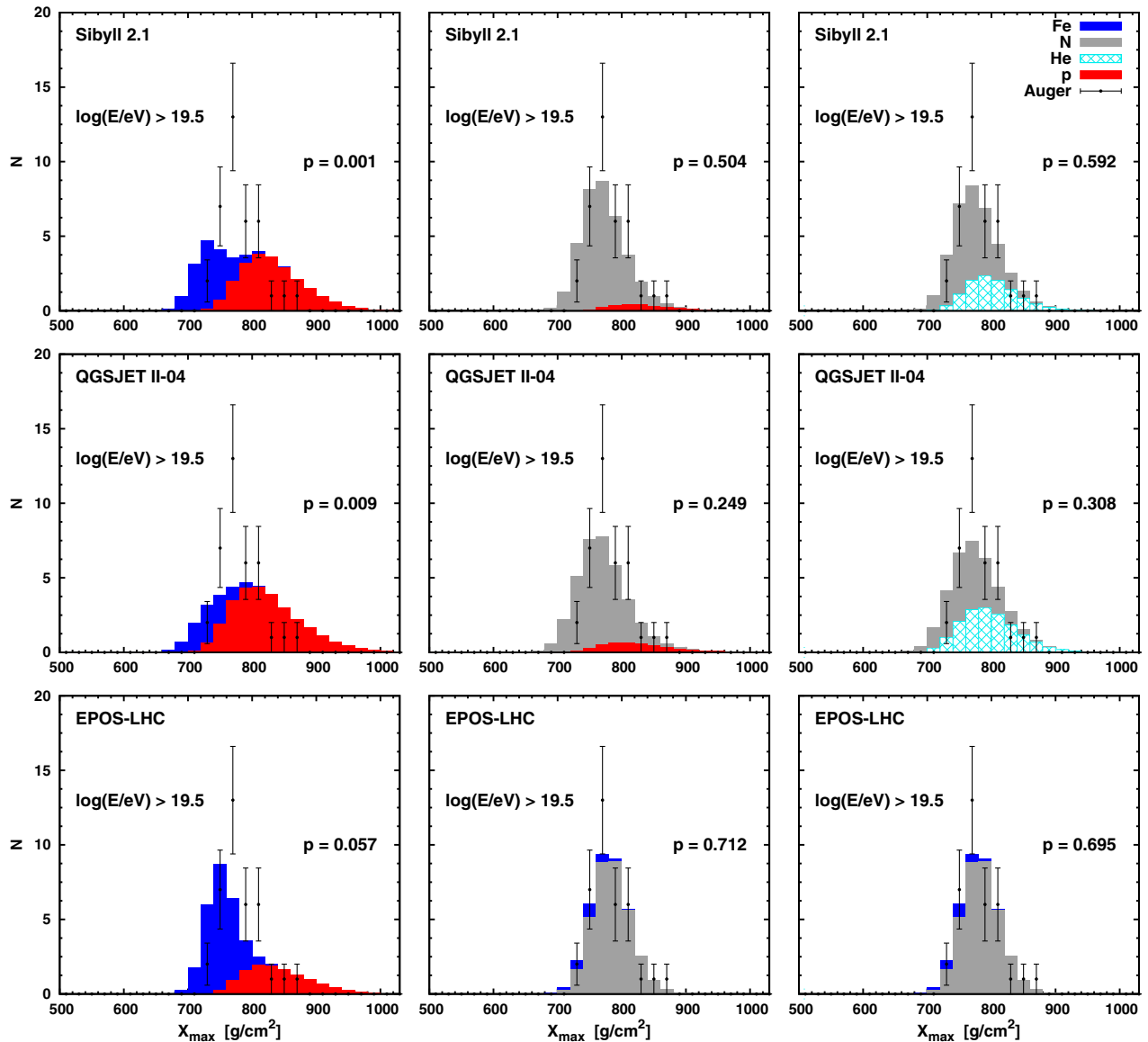

FIG. 6 (color online). X_{max} distribution of the fits for energy bin $E = 10^{19.0-19.1}$ eV. See caption to Fig. 5.

(Fig. 2), while all species fractions are shown when more than two components are considered (Figs. 3 and 4). The inner error bars are statistical and the outer ones include the systematic uncertainty added in quadrature. The p-values are shown in the lower panel of the figures, with error bars corresponding to the range of variation obtained within the systematic uncertainties. Where p-values are less than 10^{-4}, they are indicated with downward arrows.

For the simple mixture of protons and iron nuclei (Fig. 2), only the second-highest energy bin ($E = 10^{19.4-19.5}$ eV) yields good fit qualities for all three hadronic interaction models. However, the fit qualities for all three models are generally poor throughout the energy range, even when the systematic uncertainties are taken into consideration.

In order to determine whether there is any composition mixture where the models result in an adequate

representation of the data, we extended the fits to include extra components. When nitrogen nuclei are added as an intermediate mass term (Fig. 3), the quality of the fits is acceptable for EPOS-LHC. However, though much improved, the quality of the fits is still poor over most of the energy range for the other two models. p-values for all models are good for events with energy above $10^{19.2}$ eV. When helium nuclei are also included, we find that the data are well described by all models within systematic uncertainties over most of the energy range (Fig. 4).

To aid in the discussion, the X_{max} distributions of the fits are displayed for the energy bins $E = 10^{17.8-17.9}$ eV (Fig. 5), $E = 10^{19.0-19.1}$ eV (Fig. 6), and $E > 10^{19.5}$ (Fig. 7), respectively. Each figure contains nine panels that cover the species combination and hadronic interaction models used. The contributions of all species are stacked

FIG. 7 (color online). X_{max} distribution of the fits for energy bin $E > 10^{19.5}$ eV. See caption to Fig. 5.

starting from the lightest species, with the data and their statistical uncertainty superimposed. The *p*-value of the fit is included in each panel.

VI. DISCUSSION AND CONCLUSIONS

The generally poor-quality fits obtained with the two-component scenario indicate that none of the hadronic interaction models can describe the data as a simple mixture of protons and iron nuclei. The reason for the poor fits is clear when one compares the X_{max} distribution of the data with those predicted by the fits (see Figs. 5–7). The peak values for the data lie between those for protons and iron nuclei, but the distributions are too narrow to accommodate a mixture of the two. Thus, we conclude that either the model predictions are wrong or else other nuclei with shorter propagation length form a significant component of the UHECR flux that reaches the upper atmosphere.

Adding intermediate components greatly improves the fits for all hadronic interaction models. Results using EPOS-LHC in particular are satisfactory over most of the energy range. It is interesting to note that including intermediate components also brings the models into remarkable agreement in their predictions of the protons and iron nuclei contributions despite large differences in the remaining composition. This can be seen in the right column of Fig. 5. All three models give acceptable fit qualities with consistent fractions of protons, but with distinctly different predictions for the remaining composition; results of EPOS-LHC simulations favor a mixture dominated by nitrogen nuclei, while the QGSJET II-4 simulation favors helium nuclei, whereas Sibyll 2.1 modeling leads to a mixture of the two.

A substantial change in the proton fractions is observed across the entire energy range, which rises to over 60% around the ankle region ($\sim 10^{18.2}$ eV) and subsequently drops to near zero just above 10^{19} eV with a possible resurgence at higher energies. If the ankle feature is interpreted as a transition from galactic to extragalactic cosmic rays [14], the proton fraction in this energy range is surprisingly large as the upper limits on the large-scale anisotropy [15] suggest that protons with energies below $10^{18.5}$ eV are most likely produced by extragalactic sources. In order to accommodate a proton-dominated scenario for energies above 10^{18} eV [16], the hadronic interaction models would need to be modified considerably. The transition to heavier cosmic rays with increasing energy is reminiscent of a Peters cycle [17], where the maximum acceleration energy of a species is proportional to its charge Z. However, further analysis that takes into account the energy spectrum and propagation of UHECRs through the Universe would be required to confirm this. Composition-sensitive data above $10^{19.5}$ eV will be needed to allow a reliable interpretation of the observed changes of composition in terms of astrophysical models (see, e.g., Refs. [18,19]).

The absence of a significant proportion of iron nuclei in the fits is easy to understand when one looks at the X_{max} distributions for the two-component fits in Fig. 7. The X_{max} distribution of iron nuclei is predicted in all three models to peak at substantially smaller X_{max} than the data indicate. The widths of the data distributions do not allow much room to accommodate a significant contribution from iron nuclei.

Given that our analysis is limited in the number of species included, we cannot in general use the fit qualities as indicators of the validity of the hadronic interaction models. However, it is clear that the data can be described with EPOS-LHC even when restricted to the four species used in this analysis. Adding additional species will not change any conclusions with respect to this model. The QGSJET II-4 fit to the bin $E = 10^{19.0-19.1}$ eV, allowing, in principle, contributions from four species, did not in fact require any components more massive than helium nuclei. If we examine the predicted distribution (center row, right column of Fig. 6), we see that though the peak of the data distribution lines up well with that of the helium nuclei, the data distribution is too narrow to be compatible with the QGSJET II-4 prediction. Replacing the helium nuclei with a heavier species with a narrower distribution would not help the fit because its peak location would be at a value of X_{max} that is too low, and any admixture will only exacerbate the problem with the width. Since this is generally the situation wherever QGSJET II-4 has a poor fit, we conclude that adding extra species or changing the choice of species would not help to improve the fit qualities for this model.

In conclusion, we have analyzed the distributions of depths of shower maximum measured with hybrid data from Auger and found them, using current hadronic interaction models, to be inconsistent with a composition dominated by protons, nor can they support a large contribution from iron nuclei. Introducing intermediate masses to the fits produces acceptable fit qualities for some of the hadronic interaction models used. Though the fitted compositions are in general model dependent, all three models considered gave similar results for the evolution with energy of the proton fraction. However, it is still possible that the observed trend is not due to an evolution of composition mix, but rather to deviations from the standard extrapolations in hadronic interaction models.

[1] T. K. Gaisser and A. M. Hillas, in *Proceedings 15th ICRC, Plovdiv* (1977), Vol. 8, p. 353.

[2] J. Abraham *et al.* (Pierre Auger Collaboration), Phys. Rev. Lett. **104**, 091101 (2010).

[3] J. Abraham *et al.* (Pierre Auger Collaboration), Nucl. Instrum. Methods Phys. Res., Sect. A **523**, 50 (2004).

[4] A. Aab *et al.* (Pierre Auger Collaboration), Phys. Rev. D **90**, 122005 (2014).

[5] P. Abreu *et al.* (Pierre Auger Collaboration), J. Cosmol. Astropart. Phys. 02 (2013) 026.

[6] T. Bergmann, R. Engel, D. Heck, N. N. Kalmykov, S. Ostapchenko, T. Pierog, T. Thouw, and K. Werner, Astropart. Phys. **26**, 420 (2007).

[7] T. Pierog, M. K. Alekseeva, T. Bergmann, V. Chernatkin, R. Engel, D. Heck, N. N. Kalmykov, J. Moyon *et al.*, Nucl. Phys. B, Proc. Suppl. **151**, 159 (2006).

[8] K. Werner, F. M. Liu, and T. Pierog, Phys. Rev. C **74**, 044902 (2006).

[9] S. Ostapchenko, Phys. Rev. D **74**, 014026 (2006).

[10] E. J. Ahn, R. Engel, T. K. Gaisser, P. Lipari, and T. Stanev, Phys. Rev. D **80**, 094003 (2009).

[11] See, e.g., A. M. Mood and F. A. Graybill, *Introduction to the Theory of Statistics*, 2nd ed. (McGraw-Hill, New York, 1963).

[12] G. J. Feldman and R. D. Cousins, Phys. Rev. D **57**, 3873 (1998).

[13] W. A. Rolke, A. M. Lopez, and J. Conrad, Nucl. Instrum. Methods Phys. Res., Sect. A **551**, 493 (2005).

[14] J. Linsley, in *Proceedings 8th ICRC, Bombay* (1963), Vol. 4, p. 77.

[15] P. Abreu *et al.* (Pierre Auger Collaboration), Astrophys. J. Suppl. Ser. **203**, 34 (2012).

[16] V. S. Berezinsky and S. I. Grigor'eva, Astron. Astrophys. **199**, 1 (1988).

[17] B. Peters, Nuovo Cimento **22**, 800 (1961).

[18] D. Allard, Astropart. Phys. **39**, 33 (2012).

[19] A. M. Taylor, M. Ahlers, and F. A. Aharonian, Phys. Rev. D **84**, 105007 (2011).